Journal of Power Sources 196 (2011) 6828–6834

Contents lists available at ScienceDirect

Journal of Power Sources

journal homepage: www.elsevier.com/locate/jpowsour

In situ X-ray absorption spectroscopic study of Li-rich layered cathode material $Li[Ni_{0.17}Li_{0.2}Co_{0.07}Mn_{0.56}]O_2$

Atsushi Ito [a], Yuichi Sato [b], Takashi Sanada [c], Masaharu Hatano [a], Hideaki Horie [a], Yasuhiko Ohsawa [a,*]

[a] Nissan Research Center, Nissan Motor Co., Ltd., 1, Natsushima-cho, Yokosuka, Kanagawa 237-8523, Japan
[b] Department of Material and Life Chemistry, Faculty of Engineering, Kanagawa University, 3-27-1, Rokkakubashi, Kanagawa-ku, Yokohama 221-8686, Japan
[c] NISSAN ARC, LTD., 1, Natsushima-cho, Yokosuka, Kanagawa 237-0061, Japan

ARTICLE INFO

Article history:
Received 12 August 2010
Received in revised form
26 September 2010
Accepted 29 September 2010
Available online 7 October 2010

Keywords:
Cathode material
$Li[Ni_{0.17}Li_{0.2}Co_{0.07}Mn_{0.56}]O_2$
In situ X-ray absorption spectroscopy

ABSTRACT

Although Li-rich solid-solution layered materials Li_2MnO_3–$LiMO_2$ (M = Co, Ni, etc.) are expected as large capacity lithium insertion cathodes, the fundamental charge–discharge reaction mechanism of these materials is not clear. Therefore the change in valence states of Ni, Co and Mn of $Li[Ni_{0.17}Li_{0.2}Co_{0.07}Mn_{0.56}]O_2$ during charge–discharge was examined in detail using in situ X-ray absorption spectroscopy (XAS), which includes both X-ray absorption near-edge structure (XANES) and extended X-ray absorption fine structure (EXAFS) measurements. Since the Mn K edge shift during charge–discharge was not clear to determine the valence change of Mn, the Mn K pre-edge shift was examined during charge–discharge. In our measurements, only a small shift of the Mn K pre-edge toward lower energy was observed on discharge from 4.8 to 2.0 V. This corresponds to a decrease of the Mn valence from 4+ to approximately 3.6+. However, this shift cannot explain the large reversible capacity of this material and thus strongly suggests the participation of oxygen in the reversible charge–discharge reaction of this material.

1. Introduction

Recent research has focused on the Li-rich solid-solution layered cathode materials Li_2MnO_3–$LiMO_2$ (M = Co, Ni, etc.), which exhibit a discharge capacity of more than 200 mAh g^{-1} when operated above 4.6 V [1]. However, the mechanism of the charge–discharge reaction, which is the origin of the discharge capacity, has not been clarified [2–5]. There are currently two main, but controversial mechanisms proposed regarding the initial charging. The first proposed mechanism suggests that Li^+ extraction is accompanied by oxygen ejection from the cathode crystals. This is observed as oxygen gas evolution by in situ differential electrochemical mass spectroscopy (DEMS) [5]. The second proposed mechanism suggests that Li^+ extraction is not accompanied by oxygen ejection from the cathode crystals. This mechanism has been experimentally supported by a smaller weight change of the cathode during the initial charge above 4.5 V. In this mechanism, partially oxidized O^{2-} is kept inside the cathode crystals [4]. Based upon the conclusion of the first proposed mechanism, it is inferred that Mn should undertake large residual discharge capacity other than contribution from Ni and Co. However, the experimental evidence by DEMS is not quantitative. Furthermore, these cathode materials show larger capacity than theoretical values calculated based upon this mechanism [6,7]. In the second mechanism however, the highly oxidized cathode may have been gradually reduced by electrolyte solvents with insertion of a small amount of Li^+.

In order to avoid possible gradual reduction of highly oxidized cathodes, in situ X-ray absorption spectroscopy (XAS) is an appropriate method [8–13]. Transition-metal (TM) K edge XANES is typically used for this purpose. However, the shape of the Mn K edge XANES spectra for these cathode materials appears to be problematic compared to that of Ni, as will be explained in this publication. This is caused by one part of the Mn K edge XANES spectra moving in the opposite direction of the other parts during charge–discharge, near the inflection point of the Mn K edge XANES spectra. It thus appears to be somewhat complicated to discuss the valence change of Mn during charge–discharge from only the results at the Mn K edge. This study, therefore, specifically focuses on the Mn K pre-edge as we examine the change in the valence states of Ni, Co and Mn of $Li[Ni_{0.17}Li_{0.2}Co_{0.07}Mn_{0.56}]O_2$ during charge–discharge using in situ X-ray absorption spectroscopy (XAS).

2. Experimental

The preparation and characterization of $Li[Ni_{0.17}Li_{0.2}Co_{0.07}Mn_{0.56}]O_2$ using inductive-coupled plasma spectroscopy (ICP),

* Corresponding author. Tel.: +81 46 867 5199; fax: +81 46 865 5796.
E-mail address: y-oosawa@mail.nissan.co.jp (Y. Ohsawa).

0378-7753/$ – see front matter © 2010 Elsevier B.V. All rights reserved.
doi:10.1016/j.jpowsour.2010.09.105

XRD, selected area electron diffraction (SAED) and high resolution electron transmission microscopy (HRTEM) have been reported elsewhere [1,14]. A slurry containing active material, acetylene black (Denka black HS-100), and PVdF binder in a weight ratio of 60:20:20 in N-methyl-2-pyrrolidone was cast by the doctor blade method onto aluminum foil and then dried. Disks of 15 mm in diameter were punched from the cast to form cathodes. Five pouch type in situ electrochemical cells with virtually the same properties, composed of a cathode material on aluminum foil, a lithium metal anode attached to stainless-steel mesh, a micro-porous polypropylene separator, and a glass filter paper separator were made, and three of them were used to conduct in situ XAS measurements during charge–discharge. The electrolyte was 1.0 M $LiPF_6$ in ethylene carbonate/diethyl carbonate (EC/DEC, 1:2 by volume). The in situ cells were assembled in a glove box filled with dry argon. The in situ cells were cycled in the potential range of 2–4.8 V (vs. Li metal). Reference samples for non-in situ XAS measurements were prepared by mixing reference compounds with a BN powder to form disks. The XAS experiments were performed on Beam Line 14B02 of SPring-8 in Japan [15]. Two Si (1 1 1) crystals were used to monochromatize the radiation. The XAS scans that covered the Ni, Co and Mn K edges were taken in transmission mode. The REX2000 (Rigaku Corp.) and FEFF 8.2 software programs were used for the analysis of the XAS data. The back electron scattering factor and phase shift were calculated with FEFF 8.2.

The corrected Mn K pre-edge absorption structure was obtained by subtracting the background (the Voigt-fitted interpolated tail of the Mn K edge) from the observed spectra. Generally, when discussing the absorption energy shift, the peak energy is used; however, the Mn K pre-edge spectrum consists of two mutually overlapping peaks, which could be assigned as 1s to e_g (3d) and 1s to t_{2g} (3d) transitions. Thus, the two peak energies of the overlapped spectrum would be modified or difficult to determine. To avoid this, and to save time in our in situ measurements, the half-height energy of the lower energy pre-edge peak is adopted on the assumption that the lower energy peak is the same Gaussian type (with the same σ^2) across all the samples. For the purpose of visual comparison, the Mn K pre-edge spectrum is normalized with respect to the lower energy peak of the pre-edge.

3. Results and discussion

3.1. Charge and discharge curves of in situ cells

Fig. 1 shows the initial charge–discharge curves of an in situ cell at 1/20 C in the potential range between 2 and 4.8 V (vs. Li^+/Li). The charge and discharge capacities at the first cycle were 322 and 266 mAh g^{-1}, respectively. Three in situ cells, which had virtually the same properties, were used for in situ XAS measurements to save machine time of the Beam Line. In situ XAS measurements were carried out basically every 10% SOC steps, as indicated by the small arrows in Fig. 1. The notations 1-n, 2-n and 3-n represent the measurement points in the 1st charge, the 1st discharge and the 2nd charge, respectively.

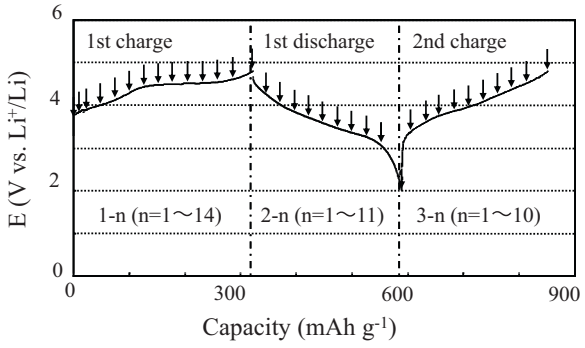

Fig. 1. The initial charge and discharge curves of an in situ cell at 1/20 C between 2 and 4.8 V vs. Li^+/Li. The small arrows correspond to measurement points. The notations 1-n, 2-n and 3-n represent the measurement points in the 1st charge, the 1st discharge and the 2nd charge, respectively.

3.2. In situ X-ray absorption near-edge structure (XANES)

3.2.1. XANES for Mn

Fig. 2 shows the normalized XANES spectra of the Mn K edge for $Li[Ni_{0.17}Li_{0.2}Co_{0.07}Mn_{0.56}]O_2$ during (a) the 1st charge, (b) the 1st discharge and (c) the 2nd charge. The numbering of all data lines is the same as Fig. 1. Fig. 2(d)–(f) shows magnifications of the pre-edge parts of Fig. 2(a)–(c), respectively. The Mn K edge consists of 3 absorptions denoted by **A**, **B** and **C**, and the Mn K pre-edge consists of 2 absorptions denoted by $\mathbf{P_1}$ and $\mathbf{P_2}$. The arrows indicate the directions of the spectrum shift during charge and discharge. Tsai et al. have reported the following assignments for these absorptions [11]. Absorption **A** is due to the electric dipole allowed transition from 1s to a 4p state with a shakedown process originating from the ligand-to-metal charge transfer (LMCT), which corresponds to the final state of $1s^1c3d^4L4p^1$, and absorption **C** is due to the electric dipole allowed transition from 1s to a 4p state without a shakedown process, which corresponds to the final state of $1s^1c3d^34p^1$. Here a 1s core hole and an oxygen 2p ligand hole are denoted by c and L, respectively. The pre-edge absorptions $\mathbf{P_1}$ and $\mathbf{P_2}$ have been assigned to the transitions from 1s to $3de_g$ and $3dt_{2g}$ for $LiMn_2O_4$ spinel compounds with a weak crystal field, respectively [16], and thus we adopted these assignments. These weak absorptions are formally electric-dipole forbidden and caused by the pure electric quadrupole coupling and/or the 3d–4p orbital mixing arising from the noncentrosymmetric environment of the slightly distorted octahedral 3a sites in rhombohetral $R\bar{3}m$ space group.

In order to evaluate the valence states of the transition metals (TMs), XANES spectra of TMs are usually compared with those of the corresponding reference compounds. Fig. 3 shows the comparison of XANES spectra at the Mn K edge for the fully charged and the fully discharged states to those for the reference Mn compounds. Based on this figure, the valence state of the Mn of the fully charged state is considered to be 4+, and the valence state of the fully discharged state is considered to be at least higher than that of Mn_2O_3 (3+) and possibly slightly higher than that of $LiMn_2O_4$ (3.5+). However, it is difficult to clearly distinguish whether the valence state of the fully discharged state is lower than that of the fully charged state, since absorption **B** shifts in the opposite direction of absorptions **A** and **C** upon discharge, as shown in Fig. 2(b). As shown in Fig. 2(a) and (c), absorption **B** also shifts in the opposite direction of absorptions **A** and **C** during the 1st charge and 2nd charge. This type of comparison may be used to understand the global shifts in the absorption edge, which occur with changes in oxidation state. The global shift of absorptions **A**, **B** and **C** is similar during the 1st charge and the 2nd charge although the valence of Mn was kept at 4+ during the 1st charge. Based on these results, it is not possible to clearly distinguish the valence change of Mn from the Mn K edge data. This finding is contradictory to previously reported works about the valence change of Mn during charge–discharge. On the other hand, the Mn K pre-edge energy does not change during the 1st charge, and changes slightly in a reversible manner during the following discharge and charge, as shown by the arrows in Fig. 2(d)–(f). Under these circumstances, we attempted to use the Mn K pre-edge absorption spectra to estimate the valence states of Mn during

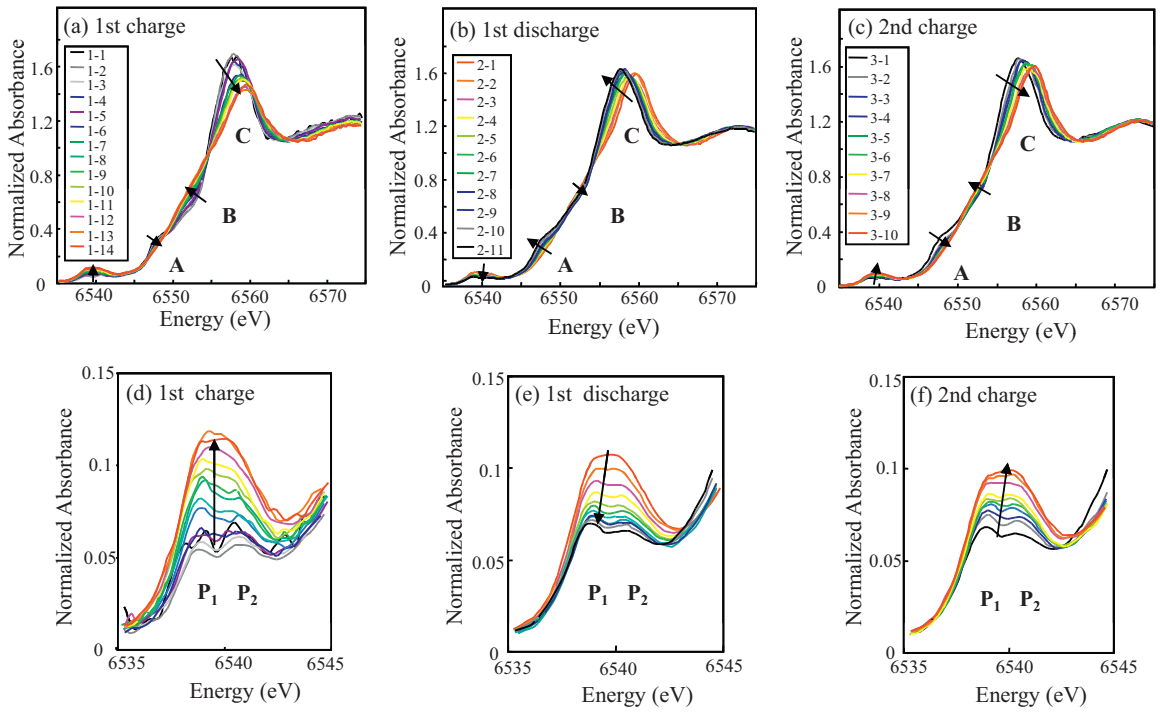

Fig. 2. Normalized XANES spectra of the Mn K edge and the Mn K pre-edge of $Li[Ni_{0.17}Li_{0.2}Co_{0.07}Mn_{0.56}]O_2$ during the initial charge–discharge. (a), (b) and (c) are those for the Mn K edge, and (d), (e) and (f) are for the Mn K pre-edge. **A**, **B** and **C** are the Mn K edge absorptions, and $\mathbf{P_1}$ and $\mathbf{P_2}$ are the Mn K pre-edge absorptions. Arrows in the figures indicate the directions of the spectrum shift during charge and discharge.

charge and discharge. The Mn K pre-edge absorption has been considered a direct measure of the valence state of the Mn atom [17,18].

Fig. 4 compares the XANES spectra for the fully charged and fully discharged states at the Mn K pre-edge to those of the reference Mn compounds. As discussed in the experimental part, each spectrum was normalized to the lower energy peak ($\mathbf{P_1}$), which is 1s to 3d e_g transition, for direct comparison among them. The spectra shown in blue and red lines are those for the fully charged and fully discharged states, respectively. The ellipsoid in the figure highlights the results indicating that the half-height energy of our cathode shifts to lower energy upon discharge. Additionally, the half-height energy of the fully discharged state is higher than those of MnO (2+), Mn_3O_4 (2.67+) and Mn_2O_3 (3+), and it is approximately the same as that of $LiMn_2O_4$ (3.5+), and lower than that of MnO_2 (4+). Although this energy shift is rather small, it is reproducible on charge and discharge as shown in Fig. 2(e) and (f).

Half-height energy values were plotted against the total capacity during charge–discharge, as shown in Fig. 5. While the data points are a little scattered during the 1st charge, the half-height energy is considered to be virtually constant since the valence state of Mn of the as-prepared material is 4+ [19] and it appears to be difficult to further oxidize octahedrally coordinated Mn (IV) within our usual potential window. The half-height energy shift upon discharge is small but appears to be larger than what could be explained by experimental error with the aid of in situ measurements. The half-height energy values for the reference Mn compounds $LiMn_2O_4$ (3.5+) and Li_2MnO_3 (4+) are also included and are shown by the dotted lines in Fig. 5. The valence state of the fully discharged state in this experiment is near that of $LiMn_2O_4$ (3.5+).

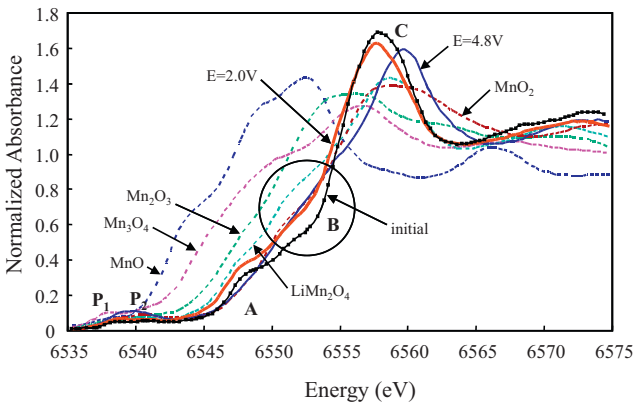

Fig. 3. Comparison between normalized XANES spectra of the Mn K edge of fully charged and fully discharged states of $Li[Ni_{0.17}Li_{0.2}Co_{0.07}Mn_{0.56}]O_2$ and those of the reference Mn compounds. The circle indicates unexpected results for the fully discharged state of the Mn valence change during charge–discharge.

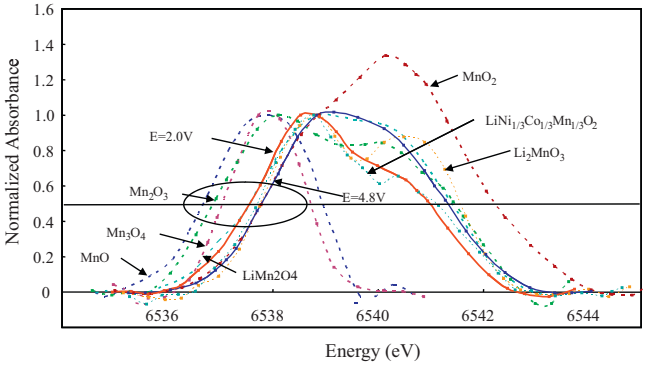

Fig. 4. Comparison between normalized XANES spectra of the Mn K pre-edge of fully charged and fully discharged states of $Li[Ni_{0.17}Li_{0.2}Co_{0.07}Mn_{0.56}]O_2$ and those of the reference Mn compounds. The background was subtracted from each spectrum, and each spectrum was normalized so that the lower-energy peak of the Mn K pre-edge became equal to unity. The data included in the ellipsoid directly compare the absorption energy of the Mn compounds.

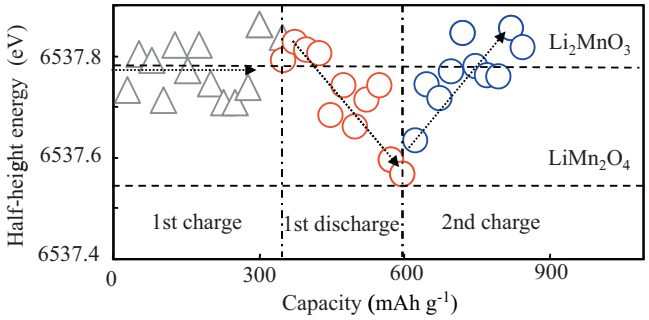

Fig. 5. Plot of photon energy at the half-height of the Mn K pre-edge vs. capacity during in situ measurements.

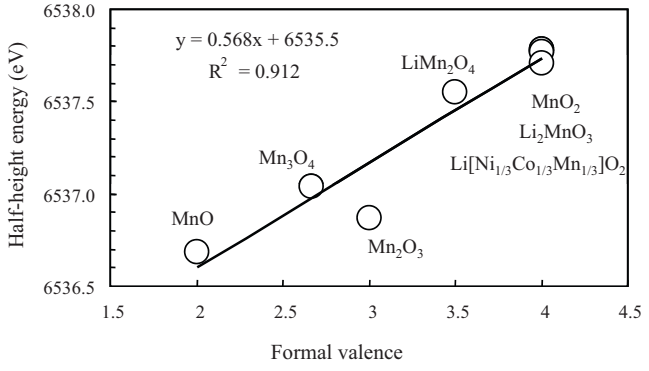

Fig. 6. Plot of half-height energy at the lower-energy end vs. formal valence for the reference Mn compounds.

Furthermore, the relation between the valence state of the Mn atom and the half-height energy of the Mn K pre-edge was verified. The half-height energy values for the reference Mn compounds were plotted against their formal valences in Fig. 6. A linear relationship was observed, except for Mn_2O_3. We believe there would be a limitation for this type of discussion since the change in ligand-field splitting energy of the Mn atom, known as the Jahn–Teller distortion, and other structural distortions could modify X-ray absorption energy. Keeping this in mind, we assumed that the linear relationship is applicable to our case, and we estimated the valence state of the fully discharged state to be approximately 3.6+ from the slope of the linear relationship. The 2nd charge was carried out to make sure of the reversible behavior of the cathode material after the 1st discharge. The change in the half-height energy during the 2nd charge was the reverse of that during the 1st discharge, and thus the reversibility of the valence change of Mn was verified.

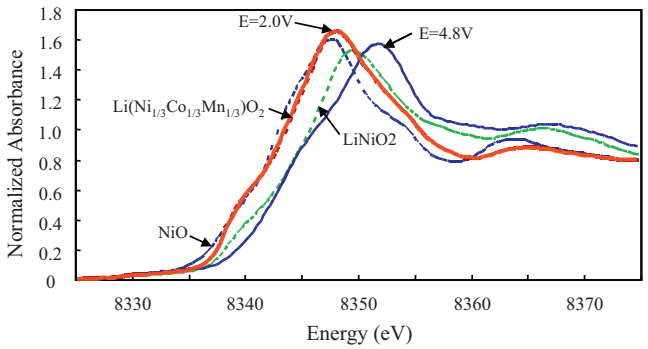

Fig. 8. Comparison between normalized XANES spectra of the Ni K edge of fully charged and fully discharged states of $Li[Ni_{0.17}Li_{0.2}Co_{0.07}Mn_{0.56}]O_2$ and those of the reference Ni compounds.

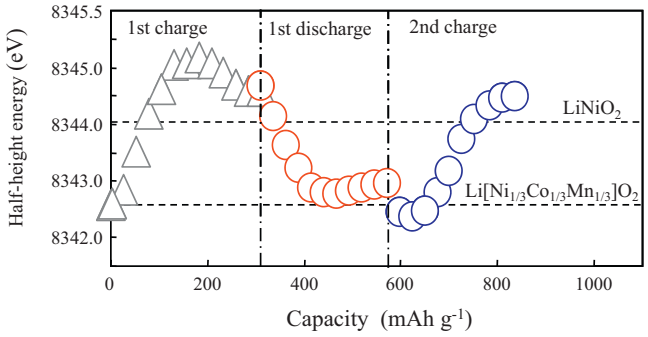

Fig. 9. Plot of photon energy at the half-height of the Ni K edge vs. capacity during in situ measurements.

3.2.2. *XANES for Ni*

Fig. 7 shows normalized XANES spectra of the Ni K edge of $Li[Ni_{0.17}Li_{0.2}Co_{0.07}Mn_{0.56}]O_2$ during the initial charge–discharge. Arrows in the figures indicate the directions of the spectrum shift during charge and discharge. Contrary to Mn, XANES spectra of the Ni K edge shift are approximately parallel during charge–discharge and thus it is not difficult to discuss the valence change during charge–discharge. Fig. 8 compares the normalized XANES spectra of the Ni K edge of the fully charged and fully discharged states of $Li[Ni_{0.17}Li_{0.2}Co_{0.07}Mn_{0.56}]O_2$ to those of the reference Ni compounds. The absorption spectrum of the fully discharged state is virtually the same as that of $Li[Ni_{1/3}Co_{1/3}Mn_{1/3}]O_2$ in which the valence state of Ni is reported to be 2+. The absorption spectrum of the fully oxidized state is higher in energy than that of $LiNiO_2$, except for the central part of lower energy side of the absorption peak, and thus its valence state is higher than that of $LiNiO_2$ (3+). Fig. 9 shows the plot of photon energy at the half-height of the

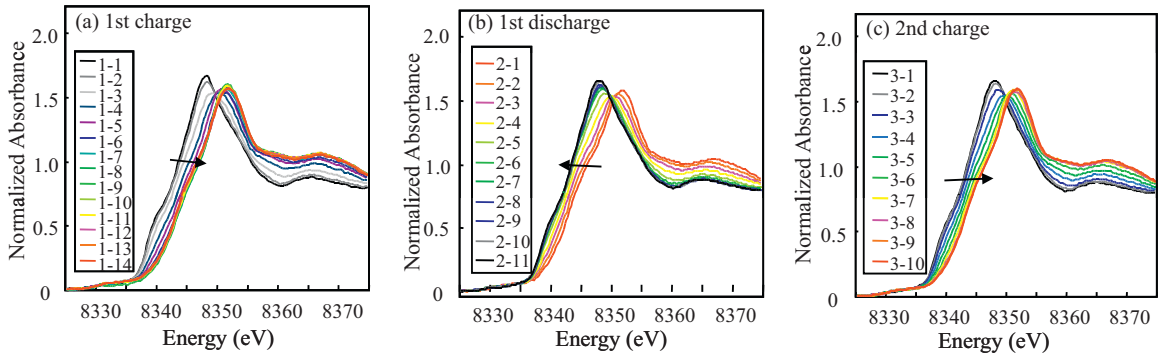

Fig. 7. Normalized XANES spectra of Ni K edge of $Li[Ni_{0.17}Li_{0.2}Co_{0.07}Mn_{0.56}]O_2$ during the initial charge–discharge. Arrows in the figures indicate the directions of the spectrum shift during charge and discharge.

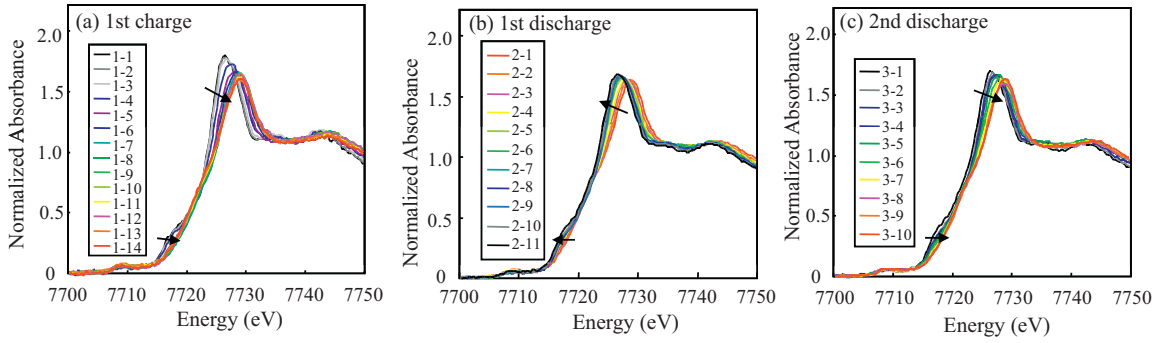

Fig. 10. Normalized XANES spectra of Co K edge of $Li[Ni_{0.17}Li_{0.2}Co_{0.07}Mn_{0.56}]O_2$ during the initial charge–discharge. Arrows in the figures indicate the directions of the spectrum shift during charge or discharge.

Ni K edge vs. capacity during in situ measurements. The highest valence of Ni at the fully charged state for this kind of cathode materials has been reported to be 3+ from the results of ex situ XANES measurements [3,4]. On the other hand, the charge compensation through the formation of Ni^{4+} has been reported [20], and in addition the larger energy shift during charge–discharge for $Li[Ni_{1/3}Co_{1/3}Mn_{1/3}]O_2$, which is expected to behave in the similar way, has been reported [11], and in both cases the contribution from the oxygen to the charge compensation was also suggested. In our case, it appears that the average oxidation state of Ni at the fully charged state is somewhere between Ni^{3+} and Ni^{4+}, likely closer to Ni^{4+}. The remaining part of the charge compensation corresponding to Ni is due to the contribution of the oxygen, most likely due to the oxygen 2p hole state by the ligand-to-metal charge transfer (LMCT).

3.2.3. XANES for Co

Fig. 10 shows the normalized XANES spectra of the Co K edge of $Li[Ni_{0.17}Li_{0.2}Co_{0.07}Mn_{0.56}]O_2$ during the initial charge–discharge. The basic change in the global pattern for Co is similar to that of Mn, as shown in Fig. 2. This similarity suggests that the environment of the Co atom is somewhat similar to that of Mn [19]. The signal to noise ratio is worse than those for Mn and Ni as a result of small quantity of Co in the cathode sample. The arrows in the figures indicate the directions of the spectrum shift during charge and discharge. Fig. 11 compares the normalized XANES spectra of the Co K edge of the fully charged and fully discharged states of $Li[Ni_{0.17}Li_{0.2}Co_{0.07}Mn_{0.56}]O_2$ to those of the reference Co compounds. The absorption spectrum of the fully discharged state is very similar to that of $LiCoO_2$, and the absorption spectrum of the fully charged state appears to be higher in energy than that of $LiCoO_2$.

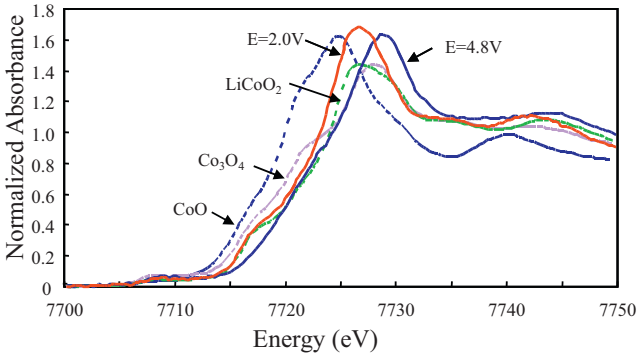

Fig. 11. Comparison of normalized XANES spectra of the Co K edge of fully charged and fully discharged states of $Li[Ni_{0.17}Li_{0.2}Co_{0.07}Mn_{0.56}]O_2$ to those of the reference Ni compounds.

3.3. In situ extended X-ray absorption fine structure (EXAFS)

3.3.1. EXAFS for Mn

The local structure of the Mn, Ni and Co ions in $Li[Ni_{0.17}Li_{0.2}Co_{0.07}Mn_{0.56}]O_2$ was measured by in situ EXAFS. Fig. 12 shows k^3-weighted Fourier transforms for the Mn absorber of $Li[Ni_{0.17}Li_{0.2}Co_{0.07}Mn_{0.56}]O_2$ during the initial charge–discharge. The notations 1-n, 2-n and 3-n correspond to the measurement points during the 1st charge, the 1st discharge and the 2nd charge, respectively. Fig. 13 shows Mn–O bond length change, estimated from in situ EXAFS measurements for $Li[Ni_{0.17}Li_{0.2}Co_{0.07}Mn_{0.56}]O_2$ during the 1st charge, the 1st discharge and the 2nd charge. A coordination number of 6 for first coordination shell was used to calculate Mn–O bond lengths. In Table 1, EXAFS data for

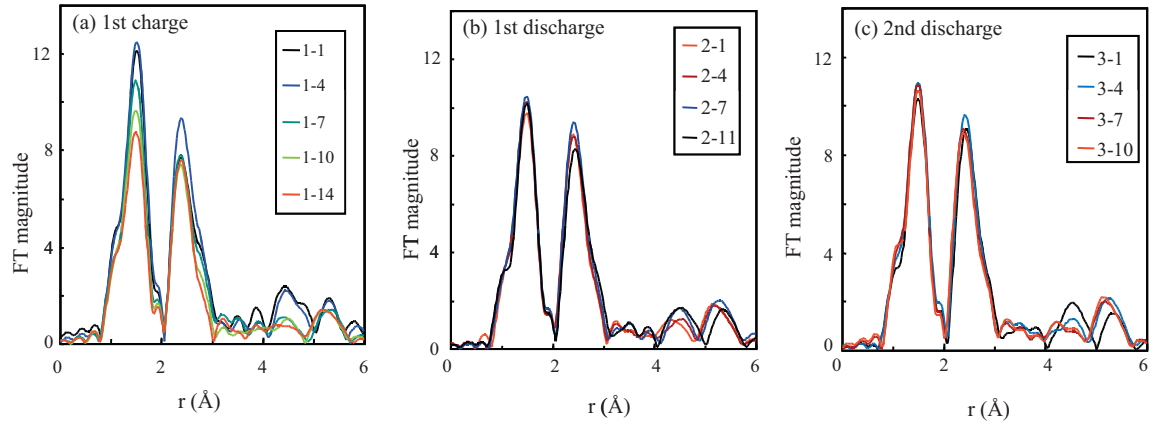

Fig. 12. k^3-Weighted Fourier transforms for the Mn absorber of $Li[Ni_{0.17}Li_{0.2}Co_{0.07}Mn_{0.56}]O_2$ during the initial charge–discharge.

Table 1
Comparison of the EXAFS results for Mn of the fully charged and fully discharged states of $Li[Ni_{0.17}Li_{0.2}Co_{0.07}Mn_{0.56}]O_2$ to those of $LiMn_2O_4$. CN: coordination number of first coordination shell, σ: Debye–Waller factor, Δk: fitting range.

Material	Mn valence	Mn–O-bond length (Å)	CN	σ^2 ($\times 10^{-3}$ Å^2)	Δk (Å^{-1})
$Li[Ni_{0.17}Li_{0.2}Co_{0.07}Mn_{0.56}]O_2$	4.8 V	1.902 ± 0.011	6	4.62	2.7–11.9
	2.0 V	1.917 ± 0.011	6	4.62	2.7–11.9
$LiMn_2O_4$[a]	3.5+	1.923	6	5.35	3–12
	Charged	1.907	6	4.05	3–12
	Discharged	1.920	6	5.08	3–12

[a] From Ref. [21].

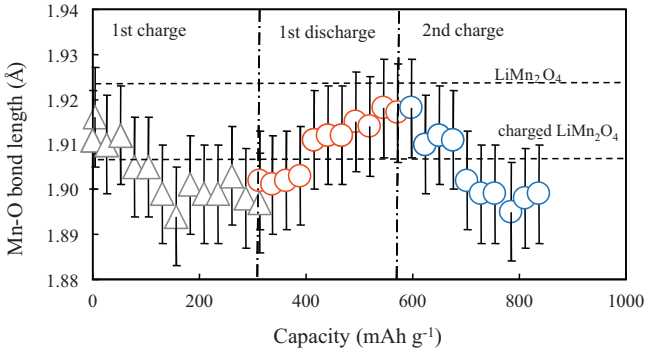

Fig. 13. Mn–O bond length change estimated from in situ EXAFS measurements for $Li[Ni_{0.17}Li_{0.2}Co_{0.07}Mn_{0.56}]O_2$ during the 1st charge, the 1st discharge and the 2nd charge.

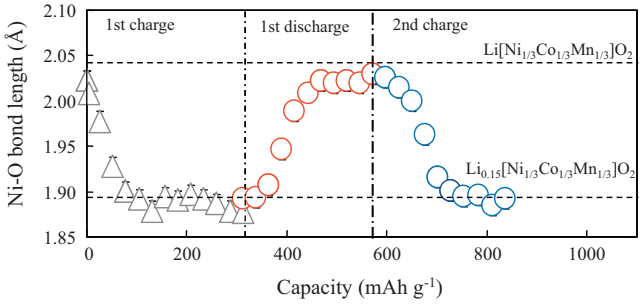

Fig. 15. Ni–O bond length change during charge–discharge. The dotted lines show the Ni–O bond lengths reported in Ref. [11].

Mn–O bond of the fully charged and fully discharged states of $Li[Ni_{0.17}Li_{0.2}Co_{0.07}Mn_{0.56}]O_2$ are compared to those of $LiMn_2O_4$ [21]. Although Mn–O bond length changes on charge and discharge are very small and only the same level as the experimental error in our EXAFS measurements, the direction and magnitude of change in Mn–O bond length is consistent with our conclusion obtained from XANES results at the Mn K pre-edge.

3.3.2. EXAFS for Ni

Fig. 14 shows k^3-weighted Fourier transforms for the Ni absorber of $Li[Ni_{0.17}Li_{0.2}Co_{0.07}Mn_{0.56}]O_2$ during the initial charge–discharge. The notations 1-n, 2-n and 3-n correspond to the measurement points in the 1st charge, the 1st discharge and the 2nd charge, respectively. Fig. 15 shows Ni–O bond length change estimated from in situ EXAFS measurements for $Li[Ni_{0.17}Li_{0.2}Co_{0.07}Mn_{0.56}]O_2$ during the 1st charge, the 1st discharge and the 2nd charge. A coordination number of 6 was used for first coordination shell to calculate Ni–O bond lengths for all data points although this is not appropriate for Ni^{3+} (Jahn–Teller ion). In Fig. 15 the Ni–O bond length values of $Li[Ni_{1/3}Co_{1/3}Mn_{1/3}]O_2$ and $Li_{0.15}[Ni_{1/3}Co_{1/3}Mn_{1/3}]O_2$ are also included and shown by the dotted lines. The valence change of the Ni for $Li[Ni_{0.17}Li_{0.2}Co_{0.07}Mn_{0.56}]O_2$ is approximately the same as that for $Li[Ni_{1/3}Co_{1/3}Mn_{1/3}]O_2$. The basic pattern of changes in energy (Fig. 9) and in bond length (Fig. 15) with capacity suggests that Ni^{4+} is reduced during the earlier stage of the 1st discharge.

3.3.3. EXAFS for Co

Fig. 16 shows k^3-weighted Fourier transforms for the Co absorber of $Li[Ni_{0.17}Li_{0.2}Co_{0.07}Mn_{0.56}]O_2$ during the initial charge–discharge. The notations 1-n, 2-n and 3-n correspond to the measurement points in the 1st charge, the 1st discharge and the 2nd charge, respectively. Fig. 17 shows Co–O bond length change estimated from in situ EXAFS measurements for $Li[Ni_{0.17}Li_{0.2}Co_{0.07}Mn_{0.56}]O_2$ during the 1st charge, the 1st discharge and the 2nd charge. In Fig. 17, the Co–O bond length values of $Li[Ni_{1/3}Co_{1/3}Mn_{1/3}]O_2$ and $Li_{0.2}[Ni_{1/3}Co_{1/3}Mn_{1/3}]O_2$ are also included and shown by the dotted lines. The valence change of the Co for $Li[Ni_{0.17}Li_{0.2}Co_{0.07}Mn_{0.56}]O_2$ is larger than that for $Li[Ni_{1/3}Co_{1/3}Mn_{1/3}]O_2$. This is likely due to the structural stability at highly charged states for our cathode.

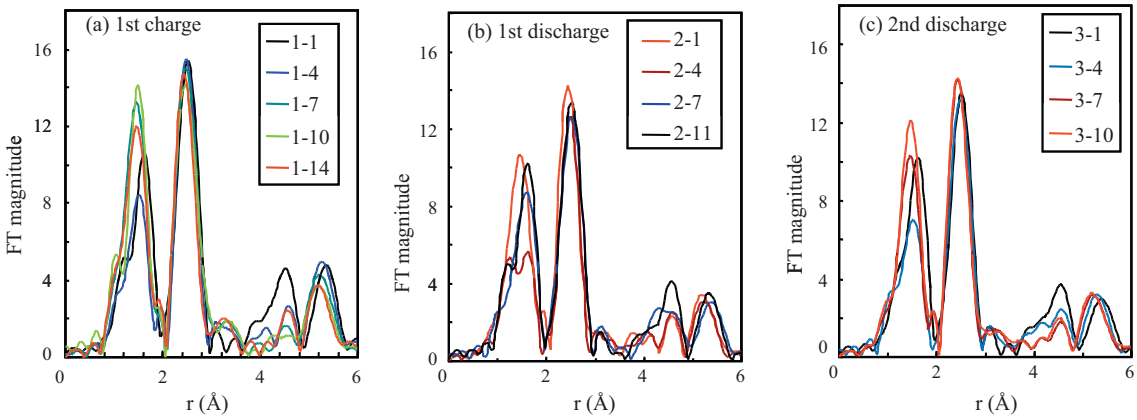

Fig. 14. k^3-Weighted Fourier transforms for the Ni absorber of $Li[Ni_{0.17}Li_{0.2}Co_{0.07}Mn_{0.56}]O_2$ during the initial charge–discharge.

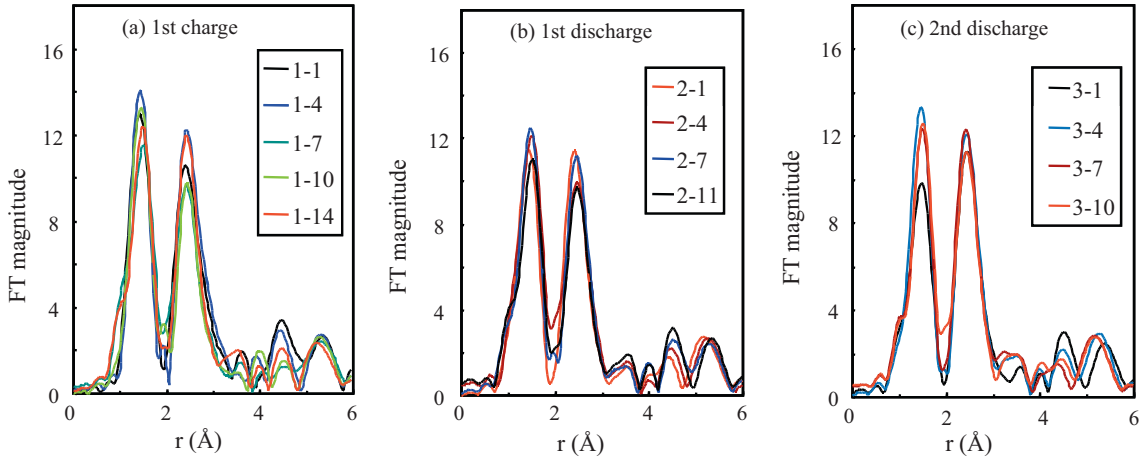

Fig. 16. k^3-Weighted Fourier transforms for the Co absorber of $Li[Ni_{0.17}Li_{0.2}Co_{0.07}Mn_{0.56}]O_2$ during the initial charge–discharge.

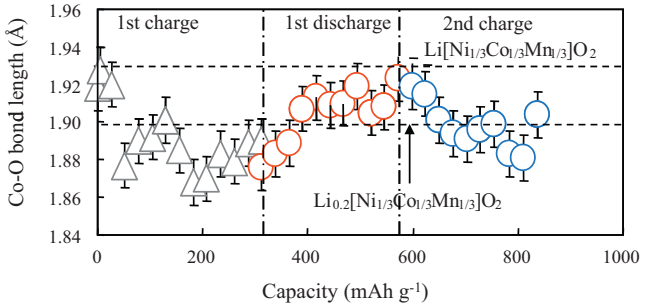

Fig. 17. Co–O bond length change during charge–discharge. The dotted lines show the Ni–O bond lengths reported in Ref. [11].

3.4. Charge compensation mechanism

Lastly, we estimated the reversible capacity of our cathode material $Li[Ni_{0.17}Li_{0.2}Co_{0.07}Mn_{0.56}]O_2$ from the valence changes of Ni, Co and Mn. To do this, we assumed that two-electron reaction for Ni, one-electron reaction for Co and 0.4-electron reaction for Mn are operative. The reversible capacity of this cathode material was estimated to be 199 mAh g^{-1}, which is much lower than the 266 mAh g^{-1} observed experimentally. Thus the large reversible capacity for our cathode cannot be explained even if the valence change of Mn observed in this experiment is taken into consideration. Therefore, another charge compensation mechanism is required. Furthermore, it is probable that contributions from Ni and Co to the reversible capacity are less than two electrons and one electron, respectively, as suggested from our XANES and EXAFS data. The most likely additional charge compensation mechanism is the participation of oxygen, probably partial oxidation of coordinated O^{2-} in the crystals, in the reversible charge–discharge reaction of our cathode material.

4. Conclusions

In situ XAS measurements were performed to examine the charge–discharge reaction mechanism of the Li-rich solid-solution layered cathode material, $Li[Ni_{0.17}Li_{0.2}Co_{0.07}Mn_{0.56}]O_2$, focusing on the Mn K pre-edge. The valence change of Mn during charge–discharge was difficult to distinguish because of the complicated energy shift of the Mn K edge absorption. Therefore, the Mn K pre-edge absorption was examined in situ. A small energy shift for the Mn K pre-edge absorption during charge–discharge was observed, and the linear relationship between the formal valence state and the Mn K pre-edge energy among the reference Mn compounds was used to estimate the valence state of Mn at the fully discharged state to be approximately 3.6+. This result is consistent with the small change observed in Mn–O bond length indicated by our in situ EXAFS data. The large reversible capacity cannot be explained even if the valence change of Mn observed in this experiment is taken into consideration. Therefore this result strongly suggests the participation of oxygen in the reversible charge–discharge reaction of our cathode material.

Acknowledgement

The authors acknowledge financial support from the Japanese New Energy and Industrial Technology Development Organization (NEDO) under the project “Development of High Performance Battery System for Next-Generation Vehicles” (Li-EAD project).

References

[1] A. Ito, D. Li, Y. Sato, M. Arao, M. Watanabe, M. Hatano, H. Horie, Y. Ohsawa, J. Power Sources 195 (2010) 567, and references cited therein.
[2] Z. Lu, J.R. Dahn, J. Electrochem. Soc. 149 (2002) A815.
[3] Y.J. Park, M.G. Kim, Y.-S. Hong, X. Wu, K.S. Ryu, S.H. Chang, Solid State Commun. 127 (2003) 509.
[4] Y.-S. Hong, Y.J. Park, K.S. Ryu, S.H. Chang, M.G. Kim, J. Mater. Chem. 14 (2004) 1424.
[5] A.R. Armstrong, M. Holzapfel, P. Novák, C.S. Johnson, S.-H. Kang, M.M. Thackeray, P.G. Bruce, J. Am. Chem. Soc. 128 (2006) 8694.
[6] C.S. Johnson, N. Li, C. Lefief, M.M. Thackeray, Electrochem. Commun. 9 (2007) 787.
[7] (a) A. Ito, Y. Ohsawa, Y. Sato, The 48th Battery Symposium in Japan, 2007, Abstract No. 1A09;
(b) Y. Yamamoto, D. Li, H. Komatsu, A. Ito, Y. Ohsawa, Y. Sato, The 49th Battery Symposium in Japan, 2008, Abstract No. 3F07.
[8] Y. Shiraishi, I. Nakai, T. Tsubata, T. Himeda, F. Nishikawa, J. Solid State Chem. 133 (1997) 587.
[9] M. Balasubramanian, J. McBreen, I.J. Davidson, P.S. Whitfield, I. Kargina, J. Electrochem. Soc. 149 (2002) A176.
[10] W.-S. Yoon, C.P. Grey, M. Balasubramanian, X.-Q. Yang, J. McBreen, Chem. Mater. 15 (2003) 3161.
[11] Y.W. Tsai, B.J. Hwang, G. Ceder, H.S. Sheu, D.G. Liu, J.F. Lee, Chem. Mater. 17 (2005) 3191.
[12] A. Deb, U. Bergmann, S.P. Cramer, E.J. Cairns, J. Appl. Phys. 97 (2005) 113523.
[13] A. Deb, U. Bergmann, S.P. Cramer, E.J. Cairns, J. Appl. Phys. 99 (2006) 063701.
[14] A. Ito, D. Li, Y. Ohsawa, Y. Sato, J. Power Sources 183 (2008) 344.
[15] http://www.spring8.or.jp/.
[16] N. Treuil, C. Labrugére, M. Menetrier, J. Portier, G. Campet, A. Deshayes, J.-C. Frison, S.-J. Hwang, S.-W. Song, J.-H. Choy, J. Phys. Chem. B 103 (1999) 2100.
[17] A. Manceau, A.I. Gorshkov, V.A. Drits, Am. Mineral 77 (1992) 1133.
[18] B. Ammundsen, D.J. Jones, J. Rozière, Chem. Mater. 8 (1996) 2799.
[19] A. Ito, Y. Sato, T. Sanada, T. Ohwaki, M. Hatano, H. Horie, Y. Ohsawa, Electrochemistry 78 (2010) 380.
[20] M.G. Kim, H.J. Shin, J.-H. Kim, S.-H. Park, Y.-K. Sun, J. Electrochem. Soc. 152 (2005) A1320.
[21] O.-S. Kwon, M.-S. Kim, K.-B. Kim, J. Power Sources 81–82 (1999) 510.